Photo-Induced Enhanced Raman from Lithium Niobate on Insulator Template

Rusul M. Al-Shammari,[1,2] Mohammad Amin Baghban,[3] Nebras Alattar,[4,5] Aoife Gowen,[4] Katia Gallo,[3] James H. Rice[1] and Brian J. Rodriguez,[1,2,]*

[1]School of Physics, University College Dublin, Belfield, Dublin 4, Ireland

[2]Conway Institute of Biomolecular and Biomedical Research, University College Dublin, Belfield, Dublin 4, Ireland

[3]Department of Applied Physics, KTH – Royal Institute of Technology, 106 91 Stockholm, Sweden

[4]School of Biosystems and Food Engineering, University College Dublin, Belfield, Dublin 4, Ireland

[5]Laser and Optoelectronics Engineering Department, University of Technology, Baghdad, Iraq

KEYWORDS. Raman, SERS, chemical enhancement, ferroelectric, photo-induced

ABSTRACT. Photo-induced enhanced Raman spectroscopy from a lithium niobate on insulator (LNOI)–silver nanoparticle template is demonstrated both by irradiating the sample with 254 nm UV light before adding an analyte and before placing the sample in the Raman system (substrate irradiation) and by irradiating the sample in the Raman system after adding

the molecule (sample irradiation). The photo-induced enhancement enables up to a ~ 7-fold increase of the surface enhanced Raman scattering signal strength of an analyte following substrate irradiation, whereas a ~ 3-fold enhancement above the surface enhanced signal is obtained for sample irradiation. The photo-induced enhancement relaxes over the course of ~ 10 hours for a substrate irradiation duration of 150 minutes before returning to initial signal levels. The increase in Raman scattering intensity following UV irradiation is attributed to photo-induced charge transfer from the LNOI template to the analyte. New Raman bands are observed following UV irradiation, the appearance of which are suggestive of a photocatalytic reaction and highlight the potential of LNOI as a photo-active SERS substrate.

INTRODUCTION

Integrated photonic sensors are promising for a wide range of applications including chemical detection, bioanalysis, and communications.[1,2] One method to increase the sensitivity of the materials used in such devices is to engineer high refractive index contrast to increase the optical path length.[3] The use of high refractive index dielectrics and refractive index contrast engineering[4,5] has been shown to increase the optical path length of the exciting light and lead to enhanced Raman scattering.[6,7] High refractive index contrast can be achieved using lithium niobate (LN) on insulator (LNOI) substrates,[4] enabling LNOI substrates to be used as photonic crystals, resonators, and sub-micron waveguides.[8,9] LN, a ferroelectric crystal widely used in photonics,[10,11] is known to be cytocompatible,[12,13] making it a suitable substrate for bio-photonic applications as well. LNOI is fabricated using He^+ ion implantation of bulk LN, wafer bonding the implanted LN surface to an SiO_2 on Si (or LN) substrate, and subsequent thermal treatment to slice out the submicron thick top LN layer from the first (implanted) LN bulk substrate.[4,14,15] The resulting LNOI structure comprises thin LN on SiO_2 on a Si (or LN) carrier wafer. Bulk LN has a refractive index of ~ 2.2.[16,17] The use of an SiO_2

interlayer with an index of refraction of ~ 1.5 [18] therefore results in a refractive index difference of ~ 0.7. Such refractive index contrast in LNOI may result in increased Raman sensitivity. It has been previously demonstrated that Raman scattering can be enhanced through multiple reflections by engineering high refractive index contrast.[6]

Another method to increase sensitivity is via surface-enhanced Raman spectroscopy (SERS). SERS enhancement is generally attributed to electromagnetic or chemical effects.[6,19,20] The electromagnetic enhancement mechanism occurs when electromagnetic waves interact with specifically-designed metallic surfaces.[19] The resultant localized surface plasmon resonances can result in SERS enhancement factors of $> 10^{10}$.[20] The polarization-dependent photochemistry of LN, which can be tailored via domain engineering[21] and chemical patterning,[22] has been previously exploited to deposit metallic nanoparticles[23–25] for Raman-based sensing of molecules.[22,26,27] To date, such work has been focused mainly on bulk single crystal LN.[10] The use of LNOI to deposit metallic nanoparticles for SERS may offer additional Raman scattering enhancement pathways, for example, through refractive index contrast effects.

Chemical enhancement typically results in an enhancement factor of $< 10^3$.[19] Several models have been proposed to explain this mechanism, depending on the specific system under study, such as the metal-to-molecule charge transfer resonance model.[19] A recent study showed that the Raman signal for an analyte can be enhanced by an order of magnitude beyond the normal electromagnetic SERS effect by ultraviolet (UV) irradiation.[28] A semiconducting TiO_2 substrate was irradiated in the absence of the analyte, prior to placing the analyte on the substrate and prior to placing the sample in the Raman system.[28] The observed photo-induced enhanced Raman spectroscopy (PIERS) was attributed to a chemical

enhancement of the SERS signal. During Raman laser excitation, electrons from defect states were reported to be promoted to the conduction band and transferred to the metallic nanoparticles.[28] Previous studies of LN-based substrates have shown that UV light influences domain engineering,[29] deposition of metallic nanoparticles,[30–32] and the wettability of LN.[33] Despite this progress, little is known about the influence of UV irradiation on Raman scattering from LN-based templates.

Here, we investigate the use of LNOI templates for Raman-based detection of molecules. PIERS from silver nanoparticles on LNOI (LNOI-Ag) is demonstrated. We show that PIERS from LNOI enables up to a ~ 7-fold increase of the SERS signal strength that persists for hours before returning to initial signal levels.

MATERIALS AND METHODS

Substrates. The following substrates were used in this work.

x-cut LNOI. A 1.0 cm × 0.5 cm thin-film LNOI-on-Si substrate (Partow Technologies LLC) with a 400 nm-thick x-cut LN layer on a 2.3 μm SiO_2 layer was used. As described elsewhere, the substrate was etched using reactive ion etching in SF_6/Ar gas to partially remove the LNOI layer.[34] Prior to etching, portions of the sample were covered with a Cr mask in order to fabricate waveguide structures unrelated to this work. The mask was subsequently removed, allowing the thickness of the remaining LNOI layer to be determined to be 130 nm using atomic force microscopy (AFM).

y-cut LNOI. A 2.0 cm × 1.0 cm y-cut LNOI substrate (Partow Technologies LLC), having regions with a completely etched LN layer (exposing the underlying SiO_2 layer) and regions that were not etched (unetched y-cut LNOI; 300 nm thick).

x-cut LN. Uniform x-cut LN (1 cm × 1 cm, 0.5 mm thick x-cut LN sample (CasTech, China)).

–z PPELN. Periodically proton exchanged LN (PPELN) was fabricated from 500 μm-thick z-cut optical grade LN (CasTech Inc., China) by selective exchange in molten benzoic acid at 200 °C through photolithographically-defined openings in a titanium mask having a period of 6.09 μm on the –z LN surface, as described previously.[22,35]

Photodeposition. Ag nanoparticles were photodeposited from $AgNO_3$ solution onto the LNOI surface. Prior to photodeposition, LNOI, LN, and PPELN samples were sonicated for 30 minutes each in acetone, isopropanol, and deionized water before being dried with compressed nitrogen. LNOI samples were placed on a glass slide, and a 70 μl volume of 0.01 M $AgNO_3$ solution was pipetted onto the sample surface. The samples were irradiated with a 254 nm above-bandgap energy (bandgap of LN ~ 3.9 eV)[36] UV lamp (11SC-2, Spectroline) located 2 cm above the surface with an average intensity of 0.92 ± 0.04 mW/cm^2 at 2 cm as measured using a light meter (HHUV254SD, Omega). The LNOI samples were irradiated for 20 minutes while the LN and PPELN samples were irradiated for 10 minutes. The resulting photogenerated electrons reduce Ag^+ to Ag^0, forming metallic nanostructures on the surface. After UV irradiation, the samples were immersed in deionized water for 1 minute and then blown dry with nitrogen. LNOI, LN, and PPELN samples were reused by cleaning them as described above with an additional step of gently rubbing the sample with lens paper soaked in isopropanol in between the acetone and isopropanol sonication steps and verifying by AFM imaging that the cleaning steps resulted in surfaces free of nanoparticles.

Atomic force microscopy. Amplitude modulation AFM (MFP-3D, Asylum Research) was employed with cantilevers having a typical resonant frequency of ~ 330 kHz and a spring constant of ~ 42 N/m (PPP-NCH, Nanosensors) to image the surface topography and measure

the surface roughness of each sample before and after photodeposition. Roughness was determined as the average roughness of three 60 μm × 60 μm images.

4-aminothiophenol. 4-aminothiophenol (4ABT) was deposited by immersing the substrates in 2 mM 4ABT in methanol solution for 15 minutes. The sample was then dipped in methanol for 5 minutes to rinse off excess 4ABT and left to dry. Raman spectroscopy was also performed on 4ABT powder (Sigma-Aldrich) on a glass slide. For Raman measurements of 4ABT powder, 2.5 mg of powder was placed on a glass slide.

Substrate irradiation. The LNOI sample with silver nanoparticles (LNOI-Ag) was irradiated under 254 nm UV light (11SC-2, Spectroline) for different time periods (30 – 150 minutes in increments of 30 minutes). The UV lamp was placed 2 cm from the substrate. After each time period, the sample was dipped in 2 mM 4ABT. Raman spectra were subsequently recorded, after which the samples were washed as previously described in order to repeat the experiment for the next irradiation time.

Sample irradiation. In this case, 4ABT was deposited on LNOI-Ag prior to irradiating the surface. The UV lamp (11SC-2, Spectroline) was placed 2 cm from the sample and positioned in order to irradiate the same location from where Raman would be measured. The LNOI surface was first irradiated with 254 nm UV light for 3 minutes, after which the lamp was turned off and Raman spectra were recorded. The UV light was subsequently turned on again to irradiate the surface for an additional 3 minutes, followed by a Raman measurement after the UV lamp was turned off. This Raman spectrum is considered as 6 minutes of sample irradiation. The on/off sequence was repeated for 84 minutes. The procedure was repeated using sub-bandgap 365 nm UV irradiation (36-380, Spectroline) with an average intensity of

0.42 ± 0.02 mW/cm^2 at 2 cm as measured using a light meter (HHUV254SD, Omega) to investigate the influence of wavelength on the Raman signal.

Raman spectroscopy. SERS spectra were collected using a 632.8 nm He–Ne excitation laser combined with a micro-spectroscopy instrumentation set-up. This consisted of a spectrograph (IsoPlane 630, Princeton Instruments) attached to back-illuminated electron multiplying charge-coupled device camera (ProEM-HS:512BX3, Princeton Instruments) and an optical microscope (IX71, Olympus) with a 10× 0.3 numerical aperture objective. All Raman spectra were recorded under the same conditions and the average spectrum of 10 measurements is displayed. Intensities are reported as the mean and standard deviation of the intensity recorded at the wavenumber of interest, as determined from 10 spectra.

Reflectance hyperspectral imaging. LNOI, LN, and PPELN substrates were investigated using visible near infrared reflectance hyperspectral imaging before and after UV irradiation using a pushbroom hyperspectral imaging system (CytoViva Inc.), comprising a 150 W halogen illumination source, an optical microscope (BX51, Olympus), with a 40×, 0.6 NA objective, coupled to an X-Y translation stage, spectrograph (Specim ImSpector V10E) and CCD detector. The UV lamp (11SC-2, Spectroline) was placed 2 cm from the sample and positioned in order to irradiate the same location to be imaged using hyperspectral imaging. The spectral data (696 × 696 spectra) were acquired from 400 nm to 1000 nm with 2 nm spectral resolution and analyzed using MATLAB (version 16b, MathWorks). Mean reflectance spectra were obtained by averaging over each pixel in the hyperspectral image. False RGB images were constructed by concatenating single wavelength reflectance images at 507, 632, and 690 nm, selected from the hyperspectral images based on the observation that reflectance changed substantially at these wavelengths after UV irradiation, and

normalizing all images to the maximum reflectance value ~ 6000 a.u. The same normalization was applied to each frame in a movie constructed from images recorded at each wavelength from 400 nm to 1000 nm.

RESULTS AND DISCUSSION

AFM topography images and representative line profiles for x-cut LNOI samples before and after Ag photodeposition are shown in Figure 1a and 1b, respectively. The Ag nanoparticles formed during the $Ag^{+} \rightarrow Ag^{0}$ reduction reaction in the presence of electrons photogenerated via irradiation with above-bandgap energy light. The surface roughness increased from 14 ± 1 nm to 18 ± 1 nm following photodeposition.

The Raman spectrum recorded for 4ABT on the x-cut LNOI substrate in the absence of Ag nanoparticles (LNOI-4ABT) (black spectrum in Figure 1c) shows a peak at 528 cm^{-1}, assigned to the underlying Si substrate.[37] The bands between 1000 and 1500 cm^{-1} are assigned to 4ABT in accordance with previous reports and as LN and SiO_2 are not Raman-active in this spectral region.[38,39] The SERS spectrum from 4ABT deposited on Ag nanoparticles assembled on x-cut LNOI (LNOI-Ag-4ABT) also shows a peak for SiO_2 (blue spectrum in Figure 1c). Other than the peak at 528 cm^{-1}, the Raman bands in the LNOI-Ag-4ABT spectrum below 1000 cm^{-1} are assigned to LN and are consistent with previously reported spectra for LNOI.[40] The intensity of these peaks is low compared to the Si peak and also to the LN peaks for x-cut LN-Ag-4ABT (Figure S1) since the LN layer is thin by comparison. The bands between 1000 and 1500 cm^{-1} are plasmon-enhanced on x-cut LNOI-Ag-4ABT by a factor of ~ 9.5, assuming both samples have the same amount of 4ABT, and show the appearance of peaks typically observed from 4ABT on Ag.[39]

Raman spectra of 4ABT powder show a series of bands with peak positions assigned to a_1 type vibrations.[38,39] The band at ~ 1583 cm^{-1} present from x-cut LNOI-Ag-4ABT and 4ABT powder (Figure 1d) corresponds to C–C stretching vibrations.[39] The three bands of 4ABT on x-cut LNOI-Ag at 1146, 1393, and 1437 cm^{-1} are chemically-enhanced b_2 mode vibrations that have previously been attributed to charge transfer and Herzberg-Teller vibronic coupling.[39,41–44] Given that the lowest unoccupied molecular orbital (LUMO) of 4ABT is 4.13 eV below the vacuum level[38,44] and that the reported work function of Ag is 4.2 eV,[45] it is likely that electrons could fill the LUMO via Raman laser excitation, having an energy of 1.96 eV.[38] Notably, these b_2 mode vibrations are also present on x-cut LNOI and x-cut LN in the absence of Ag (Figure S2). This is suggestive of a charge transfer process between LN and 4ABT as well, perhaps as a result of Raman laser excitation of electrons in surface defect states of LN,[31] as has been reported for the semiconductor ZnO.[46] Assuming similar Ag nanoparticle decoration and amount of 4ABT, the ~ 3.5-fold increase observed for LNOI could be attributed to refractive index contrast effects.

SERS spectra recorded from 4ABT on x-cut LNOI-Ag substrates that were irradiated (see Figure 2a) for 90 minutes and 160 minutes before dipping the samples into methanolic solutions of 4ABT have enhanced SERS signals (Figure 2b) compared to the spectra recorded prior to substrate irradiation (0 minutes). The enhancement increases with increased UV irradiation time. It is proposed that charge transfer of the photogenerated electrons, resulting from above-bandgap irradiation, from LNOI to Ag (work function of 4.2 eV) and 4ABT (LUMO is 4.13 eV below the vacuum level), is favorable given that the energy of the UV irradiation is 4.88 eV, higher than the energy of the Raman laser excitation. It has already been established that photogenerated electrons from LNOI will reach the LNOI surface since this is the process that leads to the deposition of Ag nanoparticles in the first place.

Furthermore, assuming a band gap of 3.9 eV,[36] an electron affinity of 1.5 eV,[47] and a Fermi level in the middle of the band gap,[31] based on reports for z-cut LN, we can estimate the work function of x-cut LNOI to be ~ 3.45 eV, which is less than the energy of the 254 nm UV irradiation. Thus, we attribute this apparent PIERS effect to a chemical enhancement of the Raman signal, beyond the electromagnetic enhancement observed in Figure 1c.[28]

The Raman intensity of the C-C stretching a_1 mode at 1583 cm^{-1} plotted as a function of substrate irradiation time shows that the signal increases by ~ 3-fold over a period of 120 minutes of UV irradiation (Figure 2d). Further irradiation resulted in a relatively minor increase in the signal. The blue-shift of the band increased with irradiation time, as shown in Figure 2d. As the photoexcited charge increases with irradiation time, the blue shift might be attributed to changes in the x-cut LNOI-Ag surface potential, which could modify the electronic levels of 4ABT.[48,49] The b_2 mode at 1437 cm^{-1} behaved similarly (Figure S3a, b, and c). Following 150 minutes of irradiation, the intensities of the band were tracked over the course of ~ 10 hours until the signals relaxed to the initial SERS values (Figure 2e). Thus, the PIERS effect lasted an order of magnitude longer than previously reported for TiO_2.[28] The more persistent PIERS process for LNOI could be explained by considering the difference in the lifetime of photoexcited charge carriers: pico- to microseconds in TiO_2 [50] and hundreds of milliseconds to tens of seconds in LN.[51] A longer lifetime provides more opportunity for charge transfer processes to take place before recombination. The photoexcited charge lifetime is likely to be further influenced by UV-induced band bending and the presence of, e.g., intrinsic defects[51,52] or those introduced during reactive ion etching.[53]

SERS spectra of x-cut LNOI-Ag-4ABT with and without sample irradiation (Figure 3a) are shown in Figure 3b. As with substrate irradiation, sample irradiation enhances the SERS

signal, in this case up to ~ 3-fold. A plot of the 1583 cm^{-1} band SERS intensity versus irradiation time for spectra recorded with sample irradiation is shown in Figure 3c. The SERS signal increased during up to ~ 35 minutes of total irradiation time, after which the signal appeared to stabilize at a reduced intensity. The difference in intensity versus background as a function of irradiation time (Figure 3d) reveals that the peak remains detectable at least over the course of 90 minutes of irradiation. As with substrate irradiation, the 1583 cm^{-1} peak blue-shifted (Figure 3d). The blue shift was more pronounced during sample irradiation: ~ 22 cm^{-1} versus ~ 4 cm^{-1} for the substrate irradiation case.[43] The increased blue shift may be related to the exposure of the 4ABT in contact with LNOI during sample irradiation that might modify molecular electronic states.[48,54] The b_2 mode at 1437 cm^{-1} behaved similarly both in terms of peak intensity and shift (Figure S3d, e, and f).

The results of both substrate irradiation and sample irradiation experiments suggest that photo-induced enhancement of Raman signals might be explained by UV-assisted charge transfer from the template to 4ABT, whereas the appearance of new b_2 mode peaks might be explained by Raman laser-assisted charge transfer and Herzberg-Teller vibronic coupling. Quite strikingly, even in the absence of Ag nanoparticles, enhanced intensity (up to ~ 2-fold) of the 1583 cm^{-1} peak is observed from x-cut LNOI-4ABT (Figure S4) after ~ 9 minutes of UV irradiation, emphasizing the critical role of LNOI in the process and demonstrating that charge transfer can take place directly between LNOI and 4ABT. The signal increased for up to ~ 9 minutes of UV irradiation; however, after ~ 20 minutes of UV irradiation, the 4ABT appeared to photodegrade.

To investigate the role of photogenerated charge on the proposed charge transfer mechanism, x-cut LNOI-Ag-4ABT was irradiated with 365 nm light having sub-bandgap energy, for

which no signal enhancement was observed (Figure 4a). In addition, PIERS was not observed from SiO_2-Ag-4ABT using 254 nm light (Figure 4b), emphasizing the critical role of LNOI and above-bandgap energy in the proposed charge transfer mechanism. In both cases, the intensity was significantly reduced, indicative of 4ABT photodegradation during Raman laser irradiation.

To further understand the proposed charge transfer mechanism, Raman spectra from uniform x-cut LN-Ag-4ABT, unetched y-cut LNOI-Ag-4ABT, and –z PPELN-Ag-4ABT samples subjected to sample irradiation were investigated (Figure S5). For uniform x-cut LN-Ag-4ABT and –z PPELN-Ag-4ABT, there was an initial increase in the 1583 cm^{-1} peak intensity compared to the background; however, PIERS was not observed, and within ~ 10 minutes of UV irradiation the signal reduced until the difference between peak intensity and background was negligible (Figure S5a and b). A delayed increase in the peak intensity compared to the background was observed for unetched y-cut LNOI-Ag-4ABT. The signal decreased within ~ 10 minutes of UV irradiation until the difference between peak intensity and background was negligible (Figure S5c). The initial increase in background-subtracted intensity might be attributed to a PIERS effect (i.e., a photo-induced chemical enhancement arising from charge transfer processes); however, the enhancement does not continue to increase with increasing UV irradiation time as observed for x-cut LNOI (Figure S5d). The absence of signal from 4ABT after ~ 10 minutes of UV irradiation from x-cut LN, y-cut LNOI, and –z PPELN is indicative of photodegradation of 4ABT, likely as a result of heating facilitated by Raman laser excitation and UV irradiation. Yan et al. have shown previously that UV irradiation can lead to substrate heating in LN.[52]

It is known that above-bandgap energy irradiation of LN produces electron-hole pairs,[36] which will subsequently recombine, become trapped at impurity or lattice defect sites,[55] or participate in a charge transfer process such as photocatalysis[56] or photodeposition.[57] Given also that charge transfer from LN to Ag or 4ABT is permitted under UV irradiation, this raises the question as to why sustained PIERS is observed on x-cut LNOI-Ag-4ABT and not on the other LN samples. While substrate cut and other factors including intrinsic and impurity defects can affect surface chemistry and the amount of photogenerated charge and the size and distribution of metal nanoparticles,[30,31,62,32,33,56–61] it is clear from this work that photodeposition occurs, and therefore photoexcited charge is present, on all substrates investigated, regardless of cut. Thus, the orientation of the LN substrate does not appear to play the dominant role in the PIERS effect.

To understand how each sample responds to UV irradiation, we must consider several factors. The LN layer in LNOI has been fabricated via ion implantation and ion beam slicing and further exposed to reactive ion etching. This processing changes the roughness and the optical properties and introduces defects.[63–66] It has been reported previously for TiO_2 that photogenerated charge trapped at defect sites could be excited by the Raman laser to facilitate PIERS.[28] In that sense, LN samples having different defect type and density would likely yield different PIERS behavior. Furthermore, there is a SiO_2 layer under the thin LN layer in LNOI, which increases the index of refraction contrast.[14] To investigate the light-material interaction for LN samples with and without index of refraction contrast and with and without reactive ion etched-induced defects, reflectance measurements were undertaken.

Mean reflectance spectra and hyperspectral images constructed from wavelengths 507, 632, and 690 nm for x-cut LNOI-Ag revealed a slight increase in reflectance after 24 minutes of

UV irradiation (Figure 5). In contrast, reflectance from unetched y-cut LNOI-Ag decreased significantly already after 6 minutes of UV irradiation (Figure S6). The multiple peaks in the reflectance spectra are attributed to interference fringes arising from multiple reflections at interfaces in the LNOI sample. In particular, the observed spectral spacing of the fringes in Figure 5 matches well, within the experimental uncertainties in thickness and refractive indices, the theoretical estimate of ~ 55 nm, corresponding to destructive interference between the reflections arising from the LN-SiO_2 and SiO_2-Si interfaces at the wavelengths of interest. This further indicates the possibility to optimize the response at specific wavelengths by careful tailoring of the multilayer structure. A movie constructed from the hyperspectral images of the x-cut LNOI-Ag surface before UV irradiation illustrates this wavelength dependence (Supplementary Movie 1). The reflectance from uniform x-cut LN-Ag (Figure S7) also decreased after 6 minutes of UV irradiation whereas the reflectance from –z PPELN-Ag remained largely unchanged following 6 minutes of UV irradiation (Figure S8). The absence of interference fringes is attributed to the bulk nature of these substrates. The mean values of reflectance spectra maxima are shown in Table 1.

Table 1. Mean values of reflectance spectra maxima as determined by peak fitting for LN samples before and after UV irradiation.

Sample	Before UV irradiation	After UV irradiation
x-cut LNOI-Ag	3094 ± 223	3224 ± 320
y-cut LNOI-Ag	3753 ± 870	1631 ± 86
x-cut LN-Ag	3033 ± 412	3107 ± 634
–z PPELN-Ag	5874 ± 420	3792 ± 208

Reflectance will depend on a number of factors including surface roughness and the amount and distribution of silver nanoparticles. Notably, the initial reflectance from y-cut LNOI-Ag is higher than from x-cut LNOI-Ag. The original y-cut LNOI surface had a roughness of 0.4

± 0.1 nm that increased to 7 ± 2 nm after Ag photodeposition. Thus, both the LNOI and LNOI-Ag surfaces are smoother for unetched y-cut LNOI than for etched x-cut LNOI templates. Furthermore, the thickness of LN in y-cut LNOI is 300 nm whereas the thickness of LN in x-cut LNOI is 130 nm. Perhaps the photoexcited charge confined in the thinner x-cut LNOI layer with a rougher surface leads to increased scattering and reflectance.[67] Thus, differences in thickness, roughness, crystallographic cut, and amount of silver might contribute to the different reflectance behavior observed. Notably, samples subjected to reactive ion etch, namely x-cut LNOI and –z PPELN, show similar reflectance behavior, pointing to a significant role of etching-related defects on the light-material interactions and suggesting that the observed PIERS effect for x-cut LNOI relies both on the etching process and the LN on SiO_2 structure.

Inspection of the Raman spectra (Figure S5) suggests that 4ABT photodegrades on the bulk samples at around ~ 5 – 10 minutes of UV irradiation. The photodegradation likely results from sample heating during Raman measurements and UV irradiation. Photodegradation also appears to occur for y-cut LNOI-Ag-4ABT at around ~ 10 minutes of UV irradiation. It is possible that increased scattering prevents photodegradation in the case of x-cut LNOI-Ag-4ABT, e.g., by limiting the heat produced. Thus, the increased scattering might act to protect the 4ABT from damage that would normally occur under UV irradiation and continuous Raman laser irradiation.[68]

Interestingly, for both substrate irradiation and sample irradiation experiments on x-cut LNOI-Ag-4ABT, increasing the irradiation time resulted in the appearance and subsequent enhancement of a new Raman band appearing at 1530 cm^{-1} following 60 minutes of substrate irradiation (Figure 2b; area highlighted in yellow) and 1525 cm^{-1} following 9 minutes of

sample irradiation (Figure 3b; area highlighted in yellow). Furthermore, a peak at ~ 1676 cm^{-1} appeared after 12 minutes of sample irradiation (Figure 3b; area highlighted in green). These bands are not present in previously reported Raman investigations of 4ABT, and their identity remains indeterminate. The appearance of these peaks might be due to a photocatalytic or photodecomposition reaction of 4ABT on LNOI-Ag with Raman laser and UV irradiation, and is a promising avenue of future research.

SUMMARY

Photo-induced enhanced Raman spectroscopy from a LNOI template with photodeposited silver nanoparticles enabled up to a ~ 7-fold increase of the surface enhanced Raman scattering signal strength of 4ABT. The enhancement decayed over the course of ~ 10 hours, which is an order of magnitude longer than previously reported for PIERS from a TiO_2-based template. The Raman enhancement, above the SERS enhancement of the silver nanoparticles, is attributed to photo-induced charge transfer from the template to 4ABT, while the increased duration is attributed to the slower recombination times for LN. New peaks at ~ 1525 cm^{-1} and ~ 1676 cm^{-1}, attributed to photocatalytic reactions, are visible following UV irradiation, highlighting the potential of the LNOI-Ag PIERS substrate to be used to monitor photo-activated processes.

ASSOCIATED CONTENT

Supporting Information. The following files are available free of charge.

Supporting Raman and reflectance measurements, Figures S1–S7 (PDF)

Movie constructed from normalized hyperspectral images of the x-cut LNOI-Ag surface before UV irradiation illustrating the wavelength dependence of the reflectance (AVI)

AUTHOR INFORMATION

Corresponding Author

*brian.rodriguez@ucd.ie

Author Contributions

The manuscript was written through contributions of all authors. All authors have given approval to the final version of the manuscript.

ACKNOWLEDGEMENTS

This publication has emanated from research conducted with the financial support of the UCD School of Physics (SIRAT – Scholarship in Research and Teaching) and UCD Research (SF1253 and SF1360). This work was also supported by the Swedish Scientific Research Council (VR 622-2010-526 and 621-2011-4040) and the ADOPT Linnaeus Centre for Advanced Optics and Photonics in Stockholm. Aoife Gowan would like to acknowledge the European Research Council (ERC-2013-StG—Proposal No. 335508—BioWater). The AFM and the Raman system used for this work were funded by Science Foundation Ireland (SFI07/IN1/B931 and SFI12/IP/1556, respectively). The authors thank Sabine Neumayer and Fengyuan Zhang for insightful discussions.

REFERENCES

(1) Passaro, V. M. N.; de Tullio, C.; Troia, B.; La Notte, M.; Giannoccaro, G.; De Leonardis, F. Recent Advances in Integrated Photonic Sensors. *Sensors* **2012**, *12* (11), 15558–15598 DOI: 10.3390/s121115558.

(2) Thomas-Peter, N.; Langford, N. K.; Datta, A.; Zhang, L.; Smith, B. J.; Spring, J. B.; Metcalf, B. J.; Coldenstrodt-Ronge, H. B.; Hu, M.; Nunn, J.; Walmsley, I. A. Integrated Photonic Sensing. *New J. Phys.* **2011**, *13* (055024), 1367–2630 DOI: 10.1088/1367-2630/13/5/055024.

(3) Bettotti, P. Hybrid Materials for Integrated Photonics. *Adv. Opt.* **2014**, *2014*, 891395 DOI: 10.1155/2014/891395.

(4) Poberaj, G.; Hu, H.; Sohler, W.; Günter, P. Lithium Niobate on Insulator (LNOI) for Micro-Photonic Devices. *Laser Photonics Rev.* **2012**, *6* (4), 488–503 DOI: 10.1002/lpor.201100035.

(5) Bogaerts, W.; Fiers, M.; Dumon, P. Design Challenges in Silicon Photonics. *IEEE J. Sel. Top. Quantum Electron.* **2014**, *20* (4), 1–8 DOI: 10.1109/JSTQE.2013.2295882.

(6) Alessandri, I.; Lombardi, J. R. Enhanced Raman Scattering with Dielectrics. *Chem. Rev.* **2016**, *116* (24), 14921–14981 DOI: 10.1021/acs.chemrev.6b00365.

(7) Wang, Y. Y.; Ni, Z. H.; Shen, Z. X.; Wang, H. M.; Wu, Y. H. Interference Enhancement of Raman Signal of Graphene. *Appl. Phys. Lett.* **2008**, *92* (4), 1–13 DOI: 10.1063/1.2838745.

(8) Baghban, M. A.; Schollhammer, J.; Errando-Herranz, C.; Gylfason, K. B.; Gallo, K. Bragg Gratings in Thin-Film $LiNbO_3$ Waveguides. *Opt. Express* **2017**, *25* (26), 32323 DOI: 10.1364/OE.25.032323.

(9) Wang, J.; Bo, F.; Wan, S.; Li, W.; Gao, F.; Li, J.; Zhang, G.; Xu, J. High-Q Lithium Niobate Microdisk Resonators on a Chip for Efficient Electro-Optic Modulation. *Opt. Express* **2015**, *23* (18), 23072 DOI: 10.1364/OE.23.023072.

(10) Weis, R. S.; Gaylord, T. K. Lithium Niobate: Summary of Physical Properties and Crystal Structure. *Appl. Phys. A Solids Surfaces* **1985**, *37* (4), 191–203 DOI: 10.1007/BF00614817.

(11) Arizmendi, L. Photonic Applications of Lithium Niobate Crystals. *Phys. Status Solidi* **2004**, *201* (2), 253–283 DOI: 10.1002/pssa.200303911.

(12) Carville, N. C.; Collins, L.; Manzo, M.; Gallo, K.; Lukasz, B. I.; Mckayed, K. K.; Simpson, J. C.; Rodriguez, B. J. Biocompatibility of Ferroelectric Lithium Niobate and

the Influence of Polarization Charge on Osteoblast Proliferation and Function. *J. Biomed. Mater. Res. - Part A* **2015**, *5*, 2540–2548 DOI: 10.1002/jbm.a.35390.

(13) Kilinc, D.; Blasiak, A.; Baghban, M. A.; Carville, N. C.; Al-Adli, A.; Al-Shammari, R. M.; Rice, J. H.; Lee, G. U.; Gallo, K.; Rodriguez, B. J. Charge and Topography Patterned Lithium Niobate Provides Physical Cues to Fluidically Isolated Cortical Axons. *Appl. Phys. Lett.* **2017**, *110* (5), 053702 DOI: 10.1063/1.4975304.

(14) Rabiei, P.; Gunter, P. Optical and Electro-Optical Properties of Submicrometer Lithium Niobate Slab Waveguides Prepared by Crystal Ion Slicing and Wafer Bonding. *Appl. Phys. Lett.* **2004**, *85* (20), 4603–4605 DOI: 10.1063/1.1819527.

(15) Rabiei, P.; Ma, J.; Khan, S.; Chiles, J.; Fathpour, S. Heterogeneous Lithium Niobate Photonics on Silicon Substrates. *Opt. Express* **2013**, *21* (21), 25573 DOI: 10.1364/OE.21.025573.

(16) Edwards, G. J.; Lawrence, M. A Temperature-Dependent Dispersion Equation for Congruently Grown Lithium Niobate. *Opt. Quantum Electron.* **1984**, *16* (4), 373–375 DOI: 10.1007/BF00620081.

(17) Jundt, D. H. Temperature-Dependent Sellmeier Equation for the Index of Refraction, n_e, in Congruent Lithium Niobate. *Opt. Lett.* **1997**, *22* (20), 1553 DOI: 10.1364/OL.22.001553.

(18) Malitson, I. H. Interspecimen Comparison of the Refractive Index of Fused Silica. *J. Opt. Soc. Am.* **1965**, *55* (10), 1205 DOI: 10.1364/JOSA.55.001205.

(19) Cialla, D.; März, A.; Böhme, R.; Theil, F.; Weber, K.; Schmitt, M.; Popp, J. Surface-Enhanced Raman Spectroscopy (SERS): Progress and Trends. *Anal. Bioanal. Chem.* **2012**, *403* (1), 27–54 DOI: 10.1007/s00216-011-5631-x.

(20) Sharma, B.; Frontiera, R. R.; Henry, A.; Ringe, E.; Van Duyne, R. P. SERS: Materials, Applications, and the Future. *Mater. Today* **2012**, *15* (1–2), 16–25 DOI: 10.1016/S1369-7021(12)70017-2.

(21) Hanson, J. N.; Rodriguez, B. J.; Nemanich, R. J.; Gruverman, A. Fabrication of Metallic Nanowires on a Ferroelectric Template via Photochemical Reaction. *Nanotechnology* **2006**, *17* (19), 4946 DOI: 10.1088/0957-4484/17/19/028.

(22) Carville, N. C.; Manzo, M.; Damm, S.; Castiella, M.; Collins, L.; Denning, D.; Weber, S. A. L.; Gallo, K.; Rice, J. H.; Rodriguez, B. J. Photoreduction of SERS-Active Metallic Nanostructures on Chemically Patterned Ferroelectric Crystals. *ACS Nano* **2012**, *6* (8), 7373–7380 DOI: 10.1021/nn3025145.

(23) Kitching, H.; Shiers, M. J.; Kenyon, A. J.; Parkin, I. P. Self-Assembly of Metallic Nanoparticles into One Dimensional Arrays. *J. Mater. Chem. A* **2013**, *1* (24), 6985 DOI: 10.1039/c3ta00089c.

(24) Dunn, S.; Sharp, S.; Burgess, S. The Photochemical Growth of Silver Nanoparticles on Semiconductor Surfaces–Initial Nucleation Stage. *Nanotechnology* **2009**, *20* (11), 115604 DOI: 10.1088/0957-4484/20/11/115604.

(25) Liu, X.; Ohuchi, F.; Kitamura, K. Patterning of Surface ElectronicProperties and Selective Silver Deposition on $LiNbO_3$ Template. *Funct. Mater. Lett.* **2008**, *01* (03), 177–182 DOI: 10.1142/S1793604708000344.

(26) Damm, S.; Carville, N. C.; Rodriguez, B. J.; Manzo, M.; Gallo, K.; Rice, J. H. Plasmon Enhanced Raman from Ag Nanopatterns Made using Periodically Poled Lithium Niobate and Periodically Proton Exchanged Template Methods. *J. Phys. Chem. C* **2012**, *116* (50), 26543–26550 DOI: 10.1021/jp310248w.

(27) Al-Shammari, R. M.; Alattar, N.; Manzo, M.; Gallo, K.; Rodriguez, B. J.; Rice, J. H. Single-Molecule Nonresonant Wide-Field Surface-Enhanced Raman Scattering from Ferroelectrically Defined Au Nanoparticle Microarrays. *ACS Omega* **2018**, *3* (3), 3165–3172 DOI: 10.1021/acsomega.7b01285.

(28) Ben-Jaber, S.; Peveler, W. J.; Quesada-Cabrera, R.; Cortés, E.; Sotelo-Vazquez, C.; Abdul-Karim, N.; Maier, S. A.; Parkin, I. P. Photo-Induced Enhanced Raman Spectroscopy for Universal Ultra-Trace Detection of Explosives, Pollutants and Biomolecules. *Nat. Commun.* **2016**, *7*, 12189 DOI: 10.1038/ncomms12189.

(29) Steigerwald, H.; Luedtke, F.; Buse, K.; Steigerwald, H.; Luedtke, F.; Buse, K. Ultraviolet Light Assisted Periodic Poling of Near-Stoichiometric, Magnesium-Doped Lithium Niobate Crystals. *Appl. Phys. Lett.* **2009**, *94* (3), 032906 DOI: 10.1063/1.3072802.

(30) Dunn, S.; Tiwari, D. Influence of Ferroelectricity on thePhotoelectric Effect of $LiNbO_3$. *Appl. Phys. Lett.* **2008**, *93* (9), 092905 DOI: 10.1063/1.2978195.

(31) Sun, Y.; Nemanich, R. J. Photoinduced Ag Deposition on Periodically Poled Lithium Niobate: Wavelength and Polarization Screening Dependence. *J. Appl. Phys.* **2011**, *109* (10), 104302 DOI: 10.1063/1.3580509.

(32) Seal, K.; Rodriguez, B. J.; Ivanov, I. N.; Kalinin, S. V. Anomalous Photodeposition of Ag on Ferroelectric Surfaces with Below-Bandgap Excitation. *Adv. Opt. Mater.* **2014**, *2* (3), 292–299 DOI: 10.1002/adom.201300380.

(33) Al-Shammari, R. M.; Manzo, M.; Gallo, K.; Rice, J. H.; Rodriguez, B. J. Tunable Wettability of Ferroelectric Lithium Niobate Surfaces: The Role of Engineered Microstructure and Tailored Metallic Nanostructures. *J. Phys. Chem. C* **2017**, *121* (12), 6643–6649 DOI: 10.1021/acs.jpcc.6b12336.

(34) Baghban, M. A.; Mahato, S. K.; Gallo, K. Low-Loss Ridge Waveguides in Thin Film Lithium Niobate-on-Insulator (LNOI) Fabricated by Reactive Ion Etching. In *Advanced Photonics 2016 (IPR, NOMA, Sensors, Networks, SPPCom, SOF)*; OSA: Washington, D.C., 2016; Vol. 2016, p ITu1A.2.

(35) Manzo, M.; Laurell, F.; Pasiskevicius, V.; Gallo, K. Two-Dimensional Domain Engineering in $LiNbO_3$ via a Hybrid Patterning Technique. *Opt. Mat. Exp.* **2011**, *1* (3), 365–371.

(36) Prokhorov, A. M.; Kuzminov, I. U. S. *Physics and Chemistry of Crystalline Lithium Niobate*; Hilger: Bristol/New York, 1990.

(37) Popovic, D. M.; Milosavljevic, V.; Zekic, A.; Romcevic, N.; Daniels, S. Raman Scattering Analysis of Silicon Dioxide Single Crystal Treated by Direct Current Plasma Discharge. *Appl. Phys. Lett.* **2011**, *98* (5), 0–3 DOI: 10.1063/1.3543838.

(38) Kim, K.; Shin, D.; Choi, J. Y.; Kim, K. L.; Shin, K. S. Surface-Enhanced Raman Scattering Characteristics of 4-Aminobenzenethiol Derivatives Adsorbed on Silver. *J. Phys. Chem. C* **2011**, *115* (50), 24960–24966 DOI: 10.1021/jp208945s.

(39) Kim, K.; Choi, J. Y.; Shin, K. S. Surface-Enhanced Raman Scattering of 4-Nitrobenzenethiol and 4-Aminobenzenethiol on Silver in Icy Environments at Liquid Nitrogen Temperature. *J. Phys. Chem. C* **2014**, *118* (21), 11397–11403 DOI: 10.1021/jp5015115.

(40) Park, Y.-B.; Min, B.; Vahala, K. J.; Atwater, H. A. Integration of Single-Crystal $LiNbO_3$ Thin Film on Silicon by Laser Irradiation and Ion Implantation-Induced Layer Transfer. *Adv. Mater.* **2006**, *18* (12), 1533–1536 DOI: 10.1002/adma.200502364.

(41) Yamamoto, Y. S.; Kayano, Y.; Ozaki, Y.; Zhang, Z.; Kozu, T.; Itoh, T.; Nakanishi, S. Single-Molecule Surface-Enhanced Raman Scattering Spectrum of Non-Resonant Aromatic Amine Showing Raman Forbidden Bands. *http://arxiv.org/abs/1610.08270* **2016**.

(42) Zhang, X.; Yu, Z.; Ji, W.; Sui, H.; Cong, Q.; Wang, X.; Zhao, B. Charge-Transfer Effect on Surface-Enhanced Raman Scattering (SERS) in an Ordered Ag NPs/4-Mercaptobenzoic Acid/TiO_2 System. *J. Phys. Chem. C* **2015**, *119* (39), 22439–22444

DOI: 10.1021/acs.jpcc.5b06001.

(43) Chenal, C.; Birke, R. L.; Lombardi, J. R. Determination of the Degree of Charge-Transfer Contributions to Surface-Enhanced Raman Spectroscopy. *ChemPhysChem* **2008**, *9* (11), 1617–1623 DOI: 10.1002/cphc.200800221.

(44) Osawa, M.; Matsuda, N.; Yoshii, K.; Uchida, I. Charge-Transfer Resonance Raman Process in Surface-Enhanced Raman-Scattering from p-Aminothiophenol Adsorbed on Silver - Herzberg-Teller Contribution. *J. Phys. Chem.* **1994**, *98* (48), 12702–12707 DOI: 10.1021/j100099a038.

(45) Mohan, S.; Subramanian, B.; Sarveswaran, G. A Prototypical Development of Plasmonic Multiferroic Bismuth Ferrite Particulate and Fiber Nanostructures and their Remarkable Photocatalytic Activity under Sunlight. *J. Mater. Chem. C* **2014**, *2* (33), 6835–6842 DOI: 10.1039/C4TC01038H.

(46) Kim, K.; Kim, K. L.; Shin, K. S. Raman Spectral Characteristics of 4-Aminobenzenethiol Adsorbed on ZnO Nanorod Arrays. *Phys. Chem. Chem. Phys.* **2013**, *15* (23), 9288 DOI: 10.1039/c3cp51204e.

(47) Yang, W.-C.; Rodriguez, B. J.; Gruverman, A.; Nemanich, R. J. Polarization-Dependent Electron Affinity of $LiNbO_3$ Surfaces. *Appl. Phys. Lett.* **2004**, *85* (12), 2316–2318 DOI: 10.1063/1.1790604.

(48) Grasseschi, D.; Toma, H. E. The SERS Effect in Coordination Chemistry. *Coord. Chem. Rev.* **2017**, *333*, 108–131 DOI: 10.1016/j.ccr.2016.11.019.

(49) Lopez-Ramirez, M. R.; Aranda Ruiz, D.; Avila Ferrer, F. J.; Centeno, S. P.; Arenas, J. F.; Otero, J. C.; Soto, J. Analysis of the Potential Dependent Surface-Enhanced Raman Scattering of p-Aminothiophenol on the Basis of MS-CASPT2 Calculations. *J. Phys. Chem. C* **2016**, *120* (34), 19322–19328 DOI: 10.1021/acs.jpcc.6b05891.

(50) Ozawa, K.; Emori, M.; Yamamoto, S.; Yukawa, R.; Yamamoto, S.; Hobara, R.; Fujikawa, K.; Sakama, H.; Matsuda, I. Electron–Hole Recombination Time at TiO_2 Single-Crystal Surfaces: Influence of Surface Band Bending. *J. Phys. Chem. Lett.* **2014**, *2* (001), 1953–1957 DOI: 10.1021/jz500770c.

(51) Tatyana Volk. *Lithium Niobate Defects, Photorefraction and Ferroelectric Switching*; Hull, R., Osgood, R. M., Parisi, J., Warlimont, H., Eds.; Series, Springer: Berlin, 2008.

(52) Yan, W.; Shi, L.; Chen, H.; Li, Y. The UV-Light-Induced Absorption in Pure $LiNbO_3$ Investigated by Varying Compositions. *J. Phys. D. Appl. Phys.* **2008**, *41*, 085410 DOI: 10.1088/0022-3727/41/8/085410.

(53) Carville, N. C.; Neumayer, S. M.; Manzo, M.; Gallo, K.; Rodriguez, B. J. Biocompatible Gold Nanoparticle Arrays Photodeposited on Periodically Proton Exchanged Lithium Niobate. *ACS Biomater. Sci. Eng.* **2016**, *2* (8), 1351–1356 DOI: 10.1021/acsbiomaterials.6b00264.

(54) Suzuki, S.; Kaneko, S.; Fujii, S.; Marqués-González, S.; Nishino, T.; Kiguchi, M. Effect of the Molecule–Metal Interface on the Surface-Enhanced Raman Scattering of 1,4-Benzenedithiol. *J. Phys. Chem. C* **2016**, *120* (2), 1038–1042 DOI: 10.1021/acs.jpcc.5b10385.

(55) Merschjann, C.; Schoke, B.; Imlau, M. Influence of Chemical Reduction on the Particular Number Densities of Light-Induced Small Electron and Hole Polarons in Nominally Pure $LiNbO_3$. *Phys. Rev. B - Condens. Matter Mater. Phys.* **2007**, *76* (8), 1–9 DOI: 10.1103/PhysRevB.76.085114.

(56) Wang, X.; Yan, W.; Zhang, Y.; Zhang, L.; Shi, L.; Meng, H.; Xuliang, W.; Hongjian, W. Threshold Effect in the Mg-Doping Dependence of the Photocatalytic Ability of $LiNbO_3$ Nanoparticles. **2016**, September, 739–745 DOI: 10.1111/jace.14571.

(57) Carville, N. C.; Neumayer, S. M.; Manzo, M.; Baghban, M.-A.; Ivanov, I. N.; Gallo, K.; Rodriguez, B. J. Influence of Annealing on the Photodeposition of Silver on Periodically Poled Lithium Niobate. *J. Appl. Phys.* **2016**, *054102*, 1–7 DOI: 10.1063/1.4940968.

(58) Neumayer, S.; Ievlev, A. V; Collins, L.; Vasudevan, R.; Baghban, M. A.; Ovchinnikova, O. S.; Jesse, S.; Gallo, K.; Rodriguez, B. J.; Kalinin, S. V. Surface Chemistry Controls Anomalous Ferroelectric Behavior in Lithium Niobate. **2018** DOI: 10.1021/acsami.8b09513.

(59) Jia, F.; Yan, W.; Wang, D.; Zhang, L.; Shi, L.; Lin, A.; Liang, G.; Li, M.; Zhang, Y.; Zhang, J.; Dong. H; Chen, G.; Chen H. Photoinduced Ag-Nanoparticle Deposition on Fe-Doped Lithium Niobate Crystals. *Opt. Mater. Express* **2014**, *4* (2), 359 DOI: 10.1364/OME.4.000359.

(60) Li, S.; Liang, G.; Zan, Z.; Shi, L.; Yan, W.; Liang, C.; Li, F. Impact of the Crystal Orientation of Fe-Doped Lithium Niobate on Photo-Assisted Proton Exchange and Chemical Etching. *Sci. Rep.* **2017**, No. November, 1–11 DOI: 10.1038/s41598-017-16454-7.

(61) Liu, X.; Kitamura, K.; Yu, Q.; Xu, J.; Osada, M.; Takahiro, N.; Li, J.; Cao, G. Tunable and Highly Reproducible Surface-Enhanced Raman Scattering Substrates Made from

Large-Scale Nanoparticle Arrays Based on Periodically Poled $LiNbO_3$ Templates. *Sci. Technol. Adv. Mater.* **2013**, *14* (5), 055011 DOI: 10.1088/1468-6996/14/5/055011.

(62) Balobaid, L.; Carville, N. C.; Manzo, M.; Collins, L.; Gallo, K.; Rodriguez, B. J. Photoreduction of Metal Nanostructures on Periodically Proton Exchanged MgO-Doped Lithium Niobate Crystals. *Appl. Phys. Lett.* **2013**, *103*, 182904.

(63) Lu, F.; Meng, M. Q.; Wang, K. M.; Liu, X. D.; Chen, H. C. Refractive Index Profiles of Ion-Implantation Waveguides Formed on Lithium Niobate and Lithium Tantalate Crystals. *Japanese J. Appl. Physics* **1997**, *36* (7 A), 4323–4325.

(64) Hu, H.; Yang, J.; Gui, L.; Sohler, W. Lithium Niobate-on-Insulator (LNOI): Status and Perspectives. *SPIE* **2012**, *8431* (1), 84311D–1 DOI: 10.1117/12.922401.

(65) Sugliani, S.; De Nicola, P.; Montanari, G. B.; Nubile, A.; Menin, A.; Mancarella, F.; Vergani, P.; Meroni, A.; Astolfi, M.; Borsetto, M.; M.; Consonni, G.; Longone, R.; Chiarini, M.; Bianconi, M.; Bentini, G. G. High Quality Surface Micromachining of $LiNbO_3$ by Ion Implantation-Assisted Etching. *Proc. SPIE* **2013**, *8612*, 86120E DOI: 10.1117/12.2002095.

(66) S. Kruszewski, J. S. Roughness Effects in Surface Enhanced Raman Scattering - Evidence for Electromagnetic and Charge Transfer Enhancement Mechanism. *Pol. Acta Phys.* **1991**, *80* (4), 611–620.

(67) Xu, C.; Zhang, J.; Xu, L.; Ma, X.; Zhao, H. Photoinduced Charge Carriers' Accumulation and its Impact on Random lasing in Nd^{3+} Doped $(Pb,La)(Zr,Ti)O_3$ Ceramics. *J. Appl. Phys.* **2017**, *121* (24), 243104 DOI: 10.1063/1.4989976.

(68) Lyndby, N. H.; Kuhl, M.; Wangpraseurt, D. Heat Generation and Light Scattering of Green Fluorescent Protein-Like Pigments in Coral Tissue. *Sci. Rep.* **2016**, *6*, 26599 DOI: 10.1038/srep26599.

Table of Contents Graphic

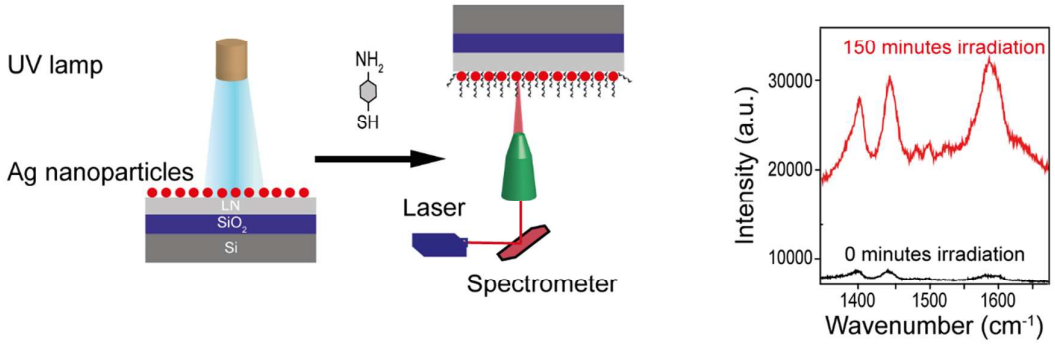

FIGURES

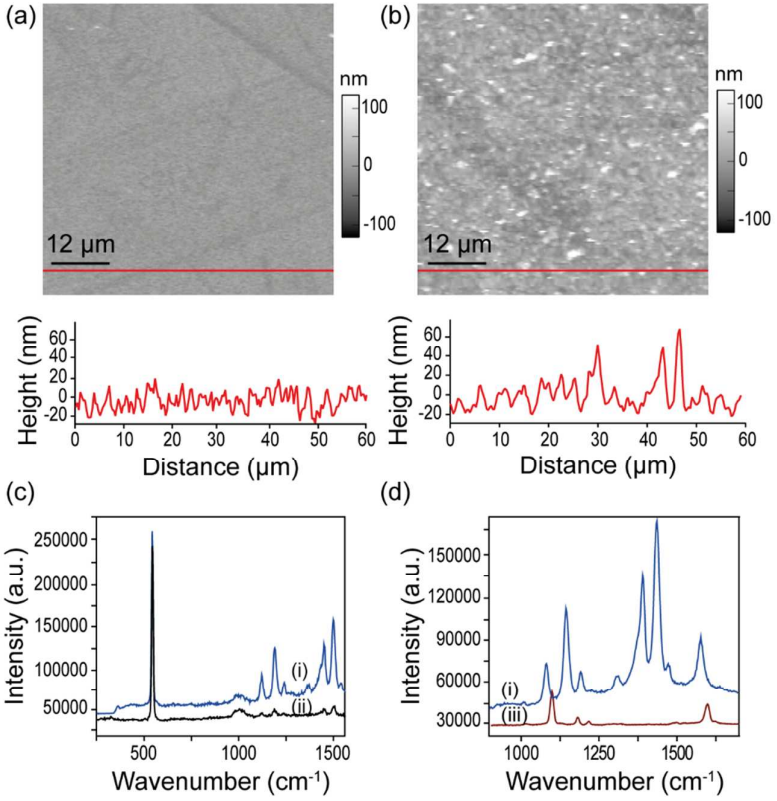

Figure 1. (a) AFM topography images and line profiles of x-cut LNOI surfaces (a) before and (b) after Ag nanoparticle deposition. (c) Raman spectra of (i) 4ABT on LNOI-Ag and (ii) 4ABT on LNOI. (d) SERS spectrum of (i) 4ABT on LNOI-Ag and Raman spectrum of (iii) 4ABT powder.

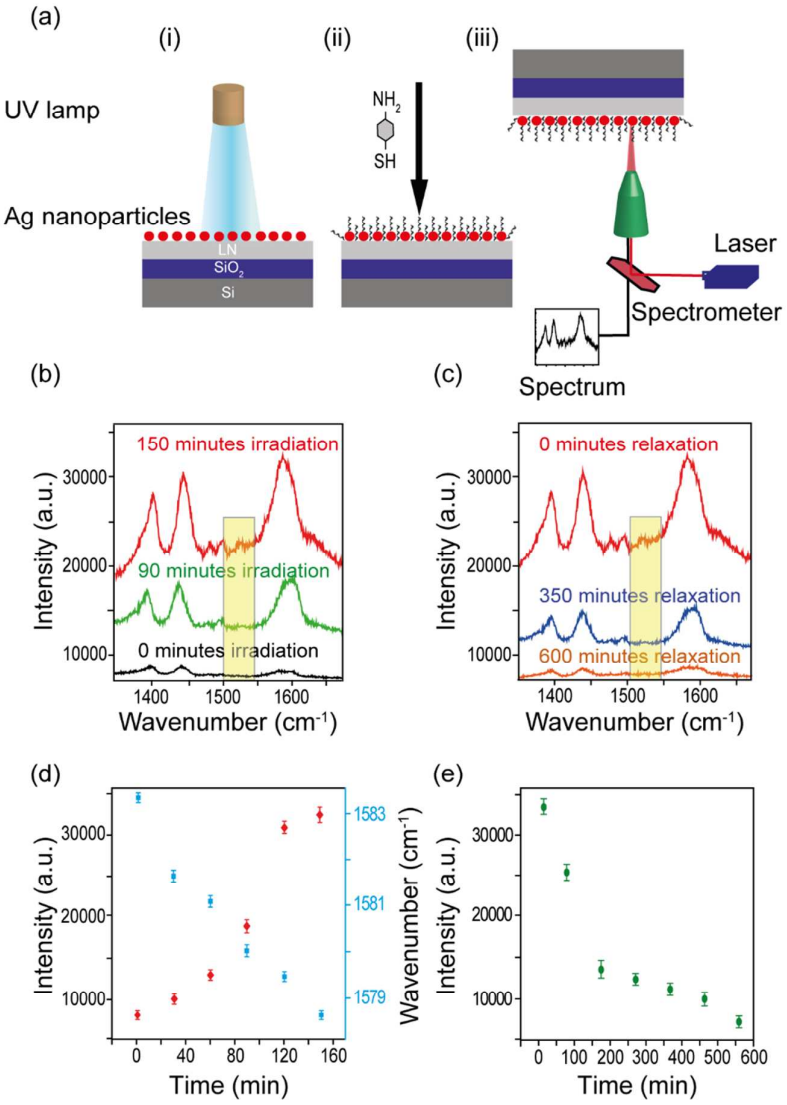

Figure 2. (a) Schematic diagram of the substrate irradiation methodology: (i) irradiation of the x-cut LNOI-Ag surface before adding 4ABT, (ii) addition of 4ABT to the substrate irradiated LNOI-Ag surface, and (iii) generation of SERS-PIERS spectra from the substrate irradiated LNOI-Ag-4ABT substrate. (b) SERS spectra of 4ABT on LNOI-Ag before irradiation and following substrate irradiation for 90 minutes (green) and 150 minutes (red). (c) Relaxation of the SERS-PIERS signal 0 minutes (red), 350 minutes (blue), and 600 minutes (purple) after irradiating the surface for 150 minutes. The yellow areas in (b) and (c) highlight a band at 1530 cm^{-1} that appears after UV irradiation. (d) Intensity (red) and shift (blue) of the 1583 cm^{-1} 4ABT band from LNOI-Ag with increasing substrate irradiation time. (e) Relaxation of the intensity of the 1583 cm^{-1} band as a function of time after 150 minutes of UV irradiation.

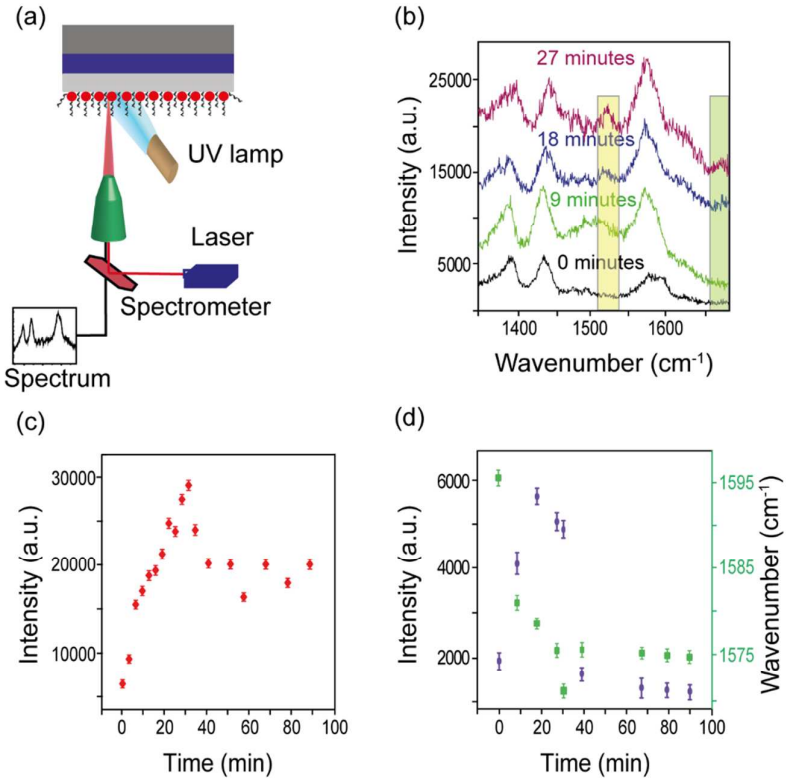

Figure 3. (a) Schematic diagram of the sample irradiation methodology. (b) SERS-PIERS spectra from x-cut LNOI-Ag-4ABT before (black) and after 9, 18, and 27 minutes of irradiation. The areas in yellow and green in (b) highlight the bands at 1530 cm^{-1} and 1676 cm^{-1} that appear after UV irradiation. (c) Intensity of the 1583 cm^{-1} band from LNOI-Ag-4-ABT with increasing irradiation time. (d) Background-subtracted intensity (purple) and shift (green) of the 1583 cm^{-1} band from LNOI-Ag-4-ABT with increasing irradiation time (full data set up to ~ 30 minutes is shown in Figure S5d).

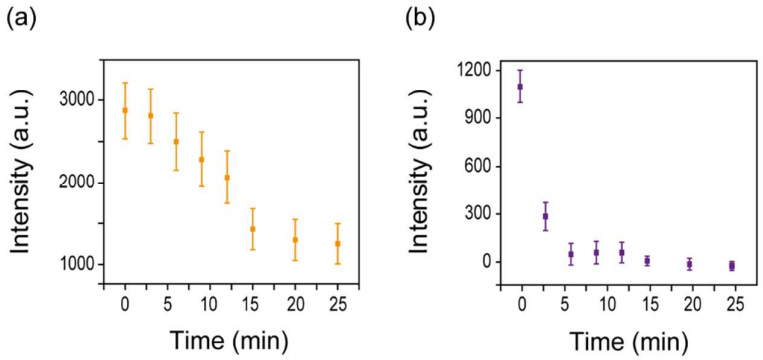

Figure 4. Background-subtracted intensity for the 1583 cm^{-1} band as a function of irradiation time from (a) x-cut LNOI-Ag-4ABT with 365 nm UV irradiation and (b) SiO_2-Ag-4ABT with 254 nm UV irradiation.

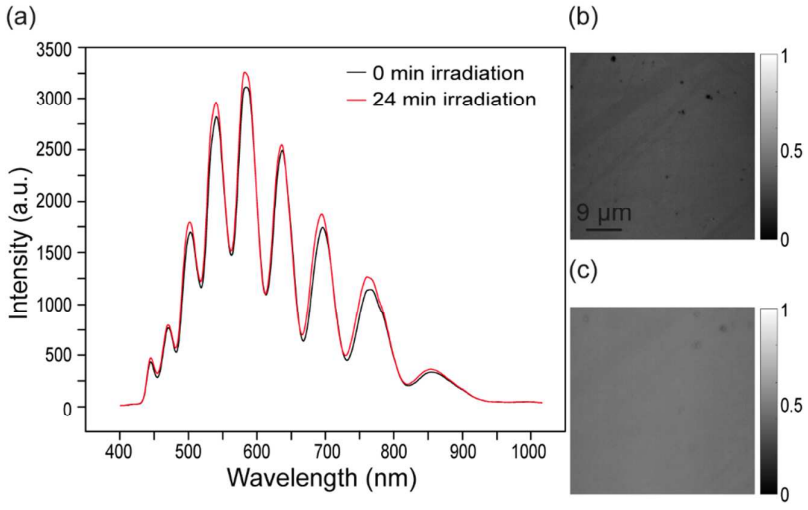

Figure 5. (a) Reflectance intensity recorded for x-cut LNOI-Ag before and after 24 minutes of UV irradiation. Normalized hyperspectral images (b) before and (c) after 24 minutes of UV irradiation.

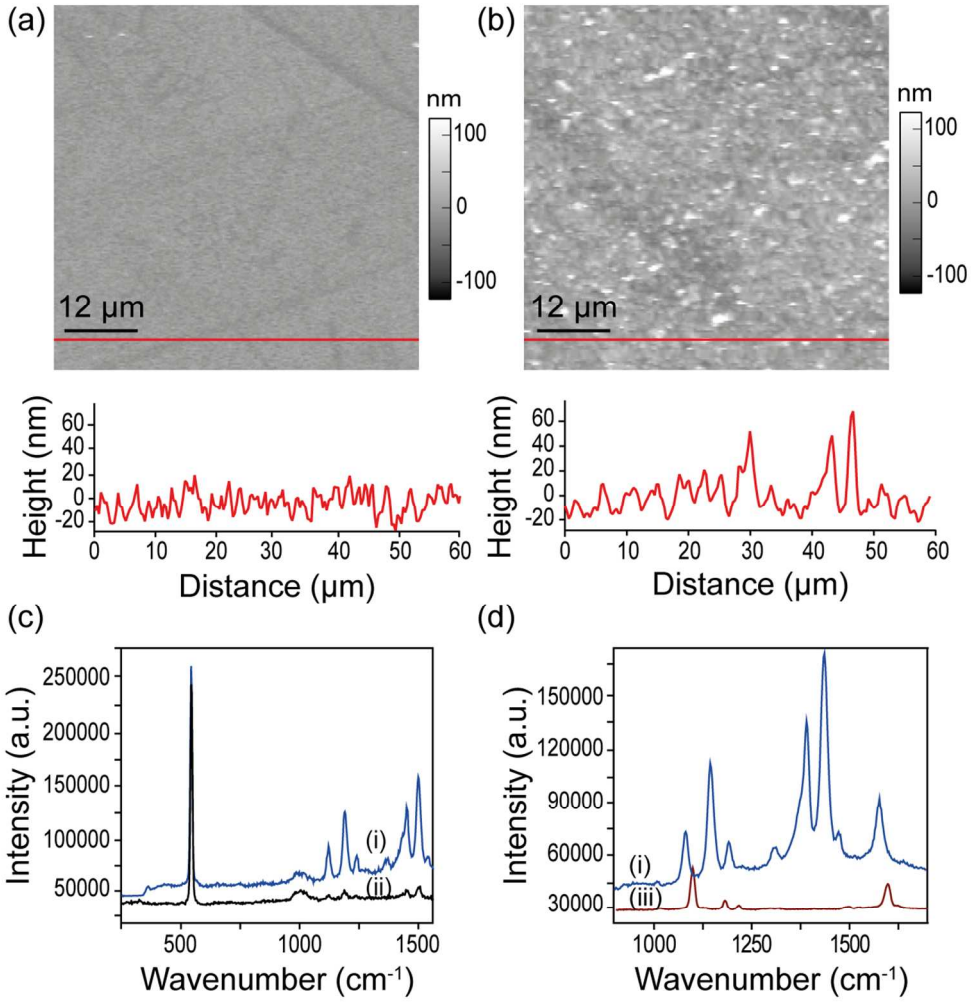

Figure 1. (a) AFM topography images and line profiles of x-cut LNOI surfaces (a) before and (b) after Ag nanoparticle deposition. (c) Raman spectra of (i) 4ABT on LNOI-Ag and (ii) 4ABT on LNOI. (d) SERS spectrum of (i) 4ABT on LNOI-Ag and Raman spectrum of (iii) 4ABT powder.

112x112mm (300 x 300 DPI)

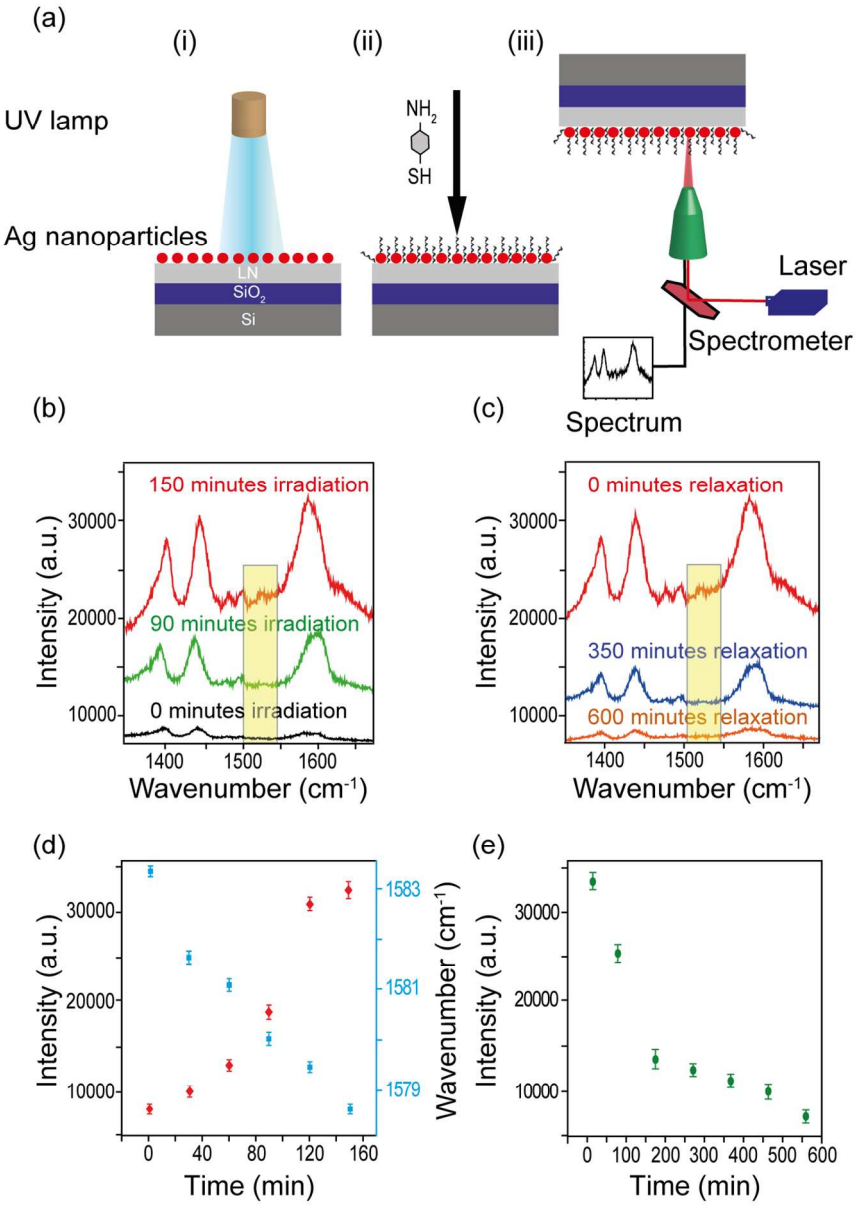

Figure 2. (a) Schematic diagram of the pre-irradiation methodology: (i) pre-irradiation of the x-cut LNOI-Ag surface before adding 4ABT, (ii) addition of 4ABT to the pre-irradiated LNOI-Ag surface, and (iii) generation of SERS-PIERS spectra from the pre-irradiated LNOI-Ag-4ABT substrate. (b) SERS spectra of 4ABT on LNOI-Ag before irradiation and following pre-irradiation for 90 minutes (green) and 150 minutes (red). (c) Relaxation of the SERS-PIERS signal 0 minutes (red), 350 minutes (blue), and 600 minutes (purple) after irradiating the surface for 150 minutes. The yellow areas in (b) and (c) highlight a band at 1530 cm-1 that appears after UV irradiation. (d) Intensity (red) and shift (blue) of the 1583 cm-1 4ABT band from LNOI-Ag with increasing pre-irradiation time. (e) Relaxation of the intensity of the 1583 cm-1 band as a function of time after 150 minutes of UV irradiation.

112x154mm (300 x 300 DPI)

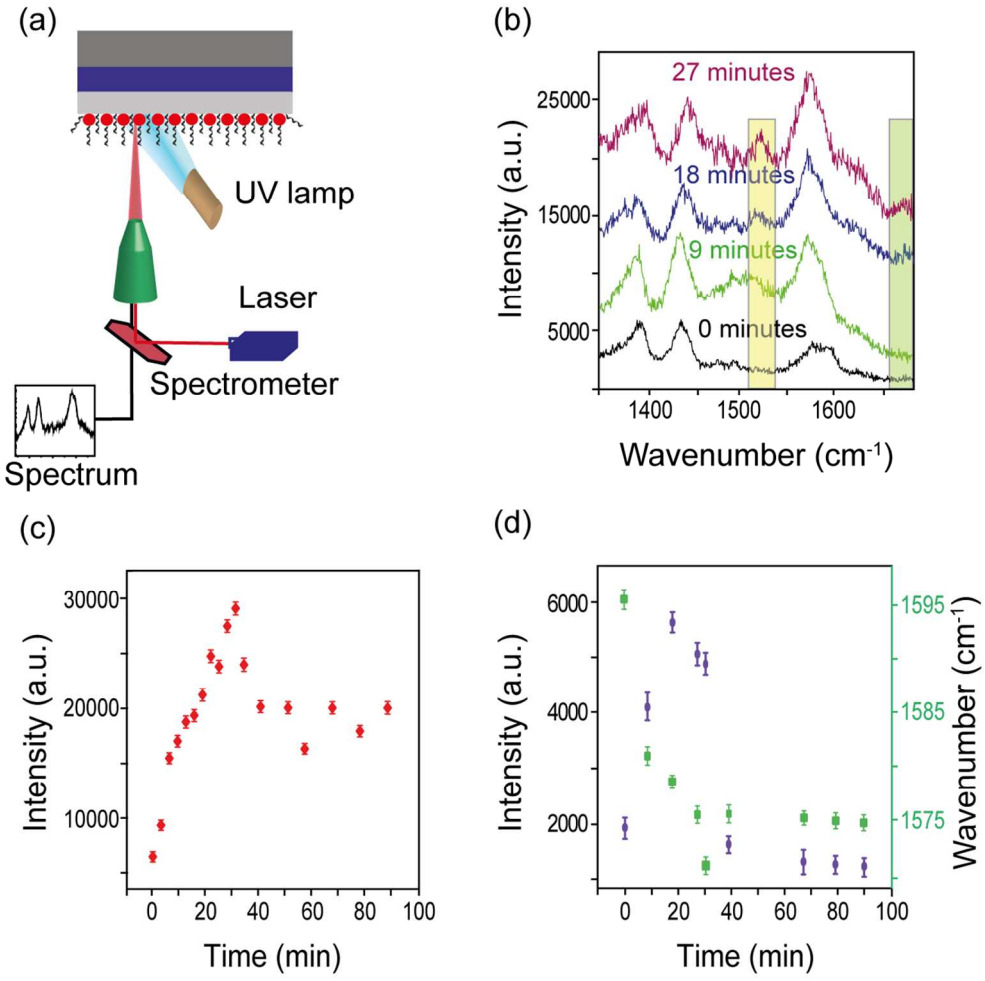

Figure 3. (a) Schematic diagram of the in-situ irradiation methodology. (b) SERS-PIERS spectra from x-cut LNOI-Ag-4ABT before (black) and after 9, 18, and 27 minutes of irradiation. The areas in yellow and green in (b) highlight the bands at 1530 cm-1 and 1676 cm-1 that appear after UV irradiation. (c) Intensity of the 1583 cm-1 band from LNOI-Ag-4-ABT with increasing irradiation time. (d) Background-subtracted intensity (purple) and shift (green) of the 1583 cm-1 band from LNOI-Ag-4-ABT with increasing irradiation time (full data set up to ~ 30 minutes is shown in Figure S5d).

112x109mm (300 x 300 DPI)

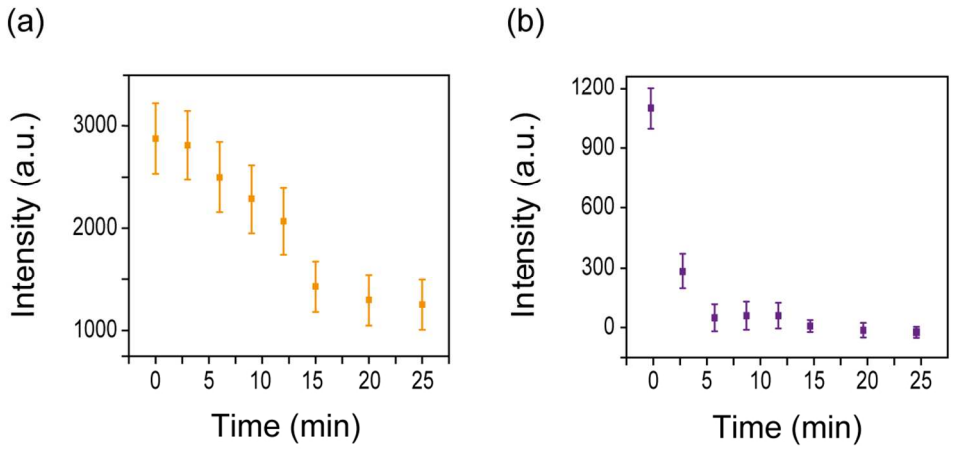

Figure 4. Background-subtracted intensity for the 1583 cm-1 band as a function of irradiation time from (a) x-cut LNOI-Ag-4ABT with 365 nm UV irradiation and (b) SiO2-Ag-4ABT with 254 nm UV irradiation.

112x52mm (300 x 300 DPI)

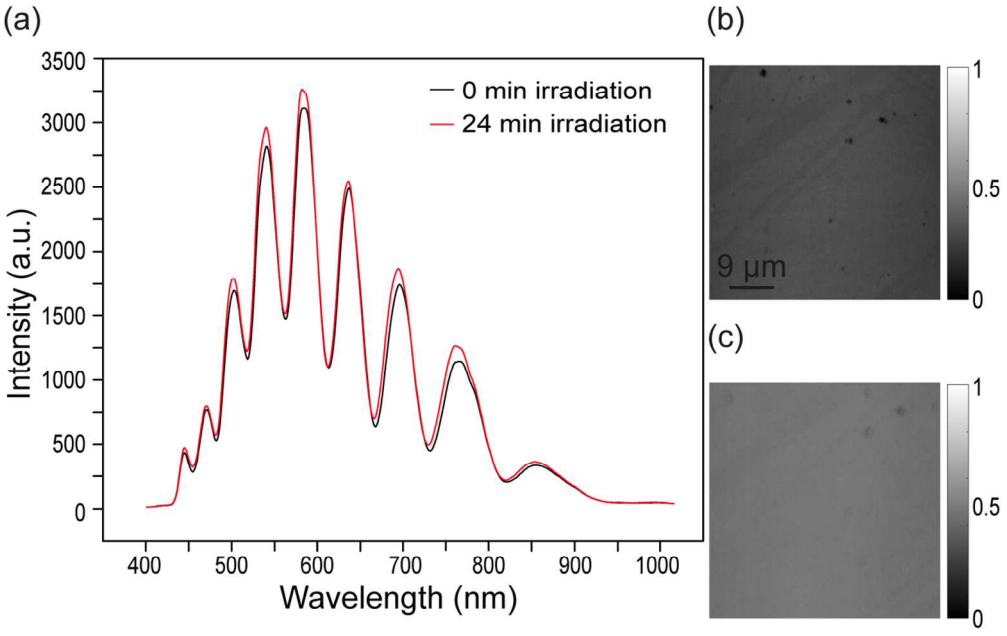

Figure 5. (a) Reflectance intensity recorded for x-cut LNOI-Ag before and after 24 minutes of UV irradiation. Normalized hyperspectral images (b) before and (c) after 24 minutes of UV irradiation.

112x72mm (300 x 300 DPI)

Supporting Information

Photoinduced Enhanced Raman from Lithium Niobate on Insulator Template

Rusul M. Al-Shammari,[1,2] Mohammad Amin Baghban,[3] Nebras Al-attar,[4,5] Aoife Gowen,[4] Katia Gallo,[3] James H. Rice[1] and Brian J. Rodriguez,[1,2,]*

[1]School of Physics, University College Dublin, Belfield, Dublin 4, Ireland

[2]Conway Institute of Biomolecular and Biomedical Research, University College Dublin, Belfield, Dublin 4, Ireland

[3]Department of Applied Physics, KTH – Royal Institute of Technology, 106 91 Stockholm, Sweden

[4]School of Biosystems and Food Engineering, University College Dublin, Belfield, Dublin 4, Ireland

[5]Laser and Optoelectronics Engineering Department, University of Technology, 10066 Baghdad, Iraq

*brian.rodriguez@ucd.ie

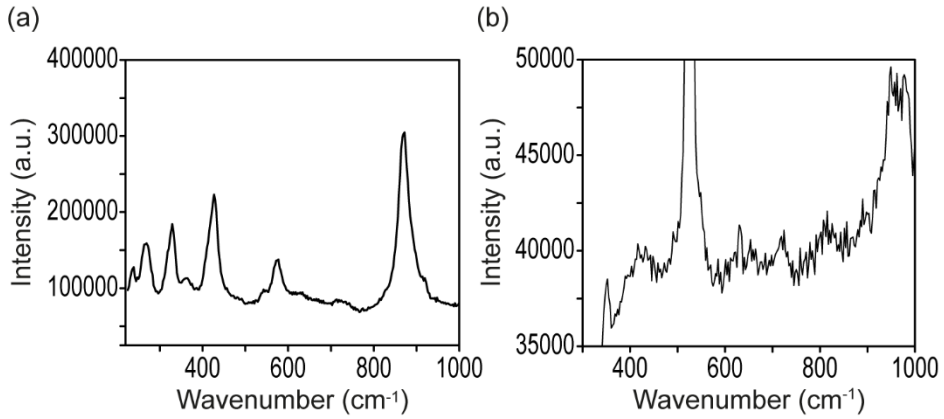

Figure S1. Raman spectra from (a) uniform x-cut LN-Ag-4ABT and (b) x-cut LNOI-Ag-4ABT. The full data range for (b) can be seen in Figure 1c(i).

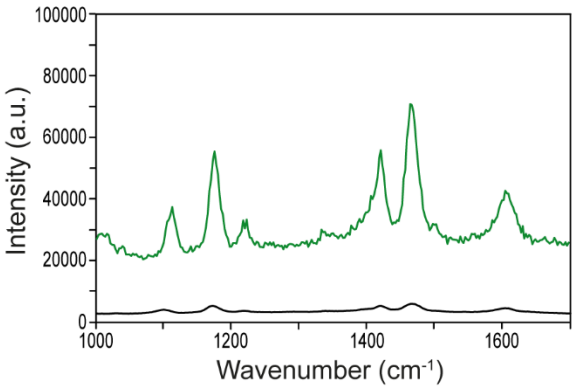

Figure S2. Raman spectra of 4ABT on x-cut LNOI (green) and on uniform x-cut LN (black) in the absence of Ag nanoparticles.

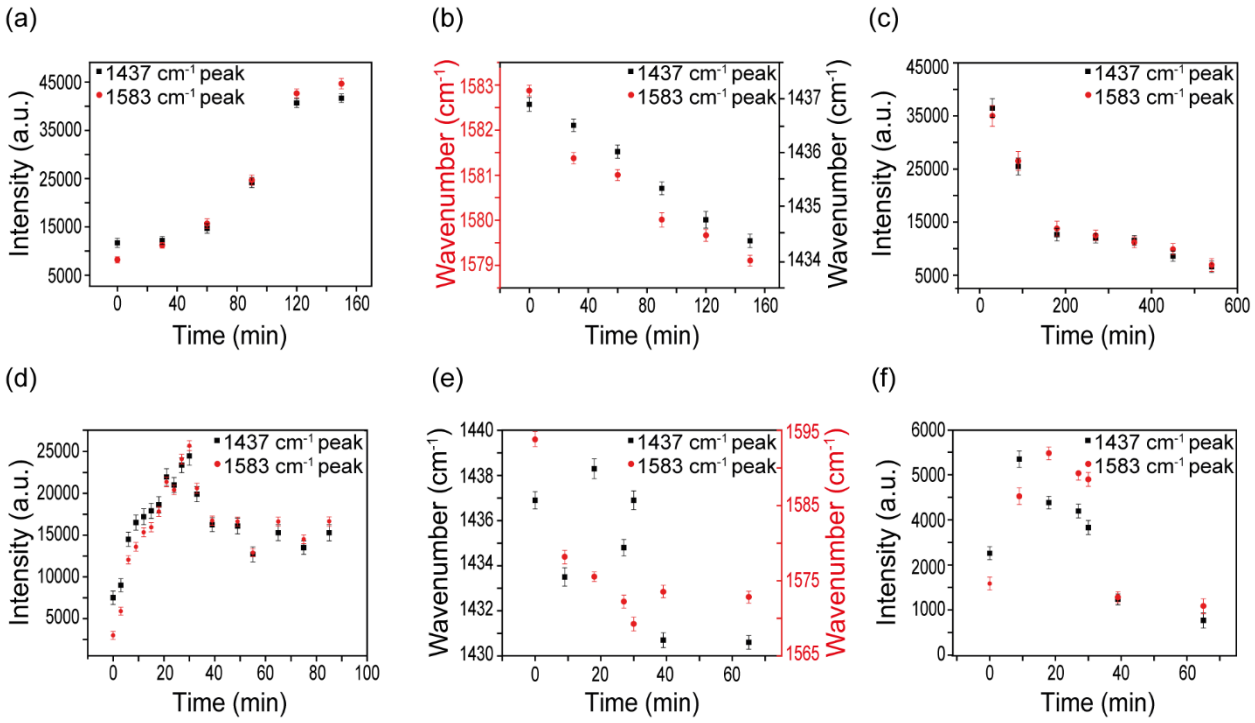

Figure S3. (a) Intensity and (b) shift of the 1583 cm^{-1} and 1437 cm^{-1} bands with increasing irradiation time for x-cut LNOI-Ag-4ABT (substrate irradiation). (c) Relaxation of the intensity of the 1583 cm^{-1} and 1437 cm^{-1} bands following 150 minutes of substrate irradiation for x-cut LNOI-Ag-4ABT. (d) Intensity and (e) shift of the 1583 cm^{-1} and 1437 cm^{-1} bands with increasing irradiation time for x-cut LNOI-Ag-4ABT (sample irradiation). (f) Background-subtracted intensity of the 1583 cm^{-1} and 1437 cm^{-1} bands with increasing sample irradiation time for x-cut LNOI-Ag-4ABT.

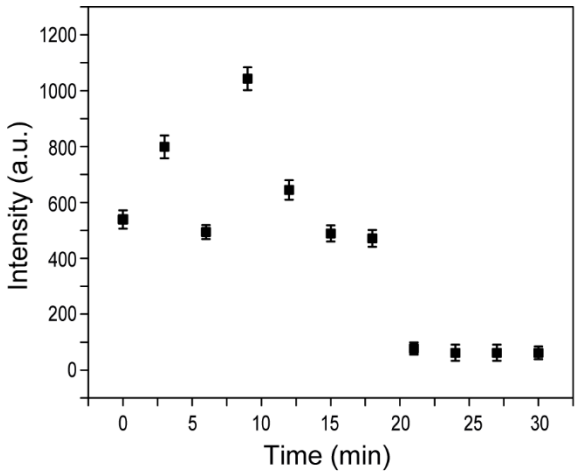

Figure S4. Background-subtracted intensity for the 1583 cm^{-1} band for sample irradiation for x-cut LNOI-4ABT without Ag nanoparticles.

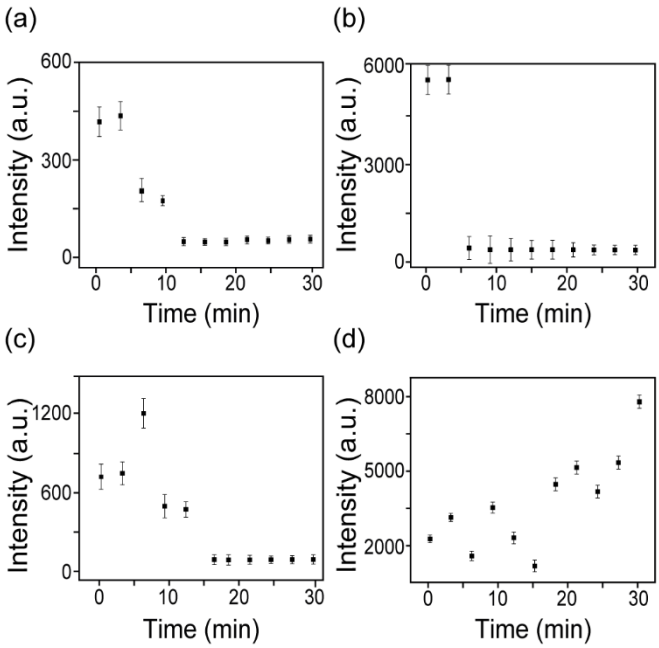

Figure S5. Background-subtracted intensity for the 1583 cm^{-1} band for sample irradiation for (a) uniform x-cut LN-Ag-4ABT, (b) –z PPELN-Ag-4ABT, (c) unetched y-cut LNOI-Ag-4ABT, and (d) etched x-cut LNOI-Ag-4ABT.

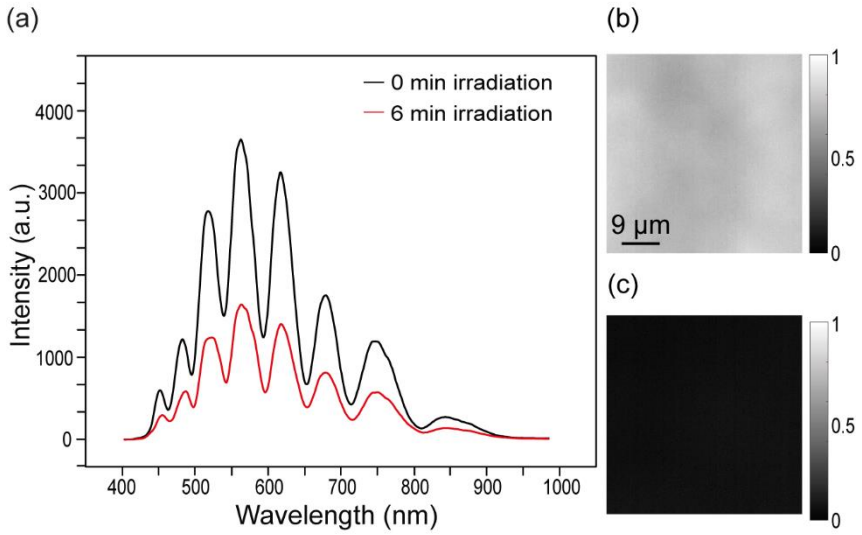

Figure S6. (a) Reflectance intensity recorded for unetched y-cut LNOI-Ag before and after 6 minutes of UV irradiation. Normalized hyperspectral images (b) before and (c) after 6 minutes of UV irradiation.

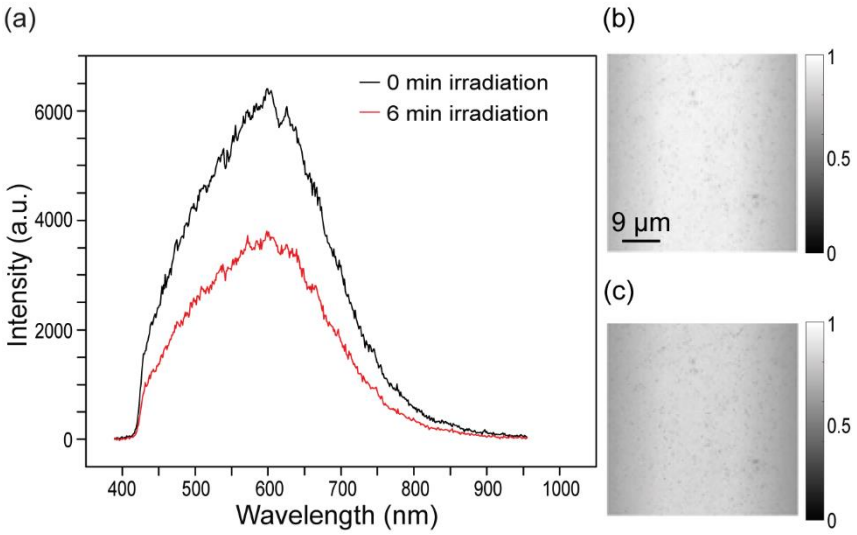

Figure S7. (a) Reflectance intensity recorded for uniform x-cut LN-Ag before and after 6 minutes of UV irradiation. Normalized hyperspectral images (b) before and (c) after 6 minutes of UV irradiation.

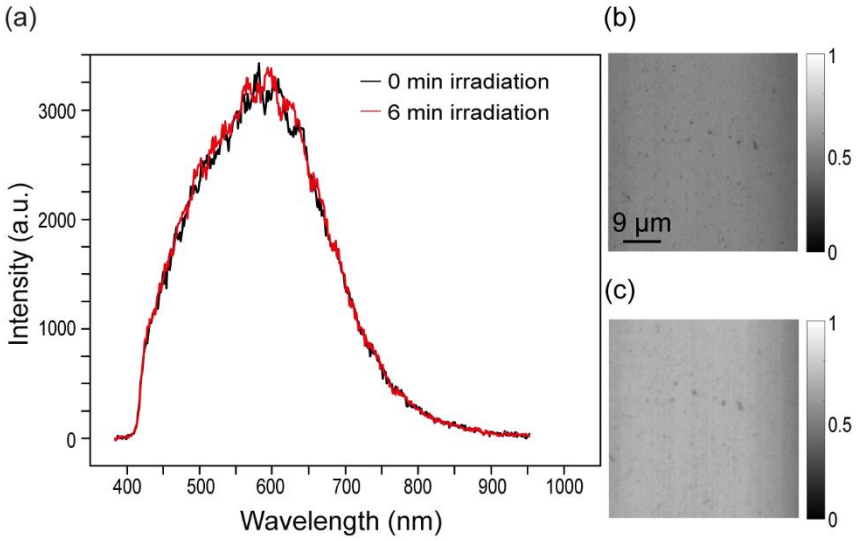

Figure S8. (a) Reflectance intensity recorded for –z PPELN before and after 6 minutes of UV irradiation. Normalized hyperspectral images (b) before and (c) after 6 minutes of UV irradiation.